RESEARCH ARTICLE

IVIM–DKI for differentiation between prostate cancer and benign prostatic hyperplasia: comparison of 1.5 T vs. 3 T MRI

Archana Vadiraj Malagi[1] · Arjunlokesh Netaji[2] · Virendra Kumar[3] · Esha Baidya Kayal[1] · Kedar Khare[4] ·
Chandan Jyoti Das[2] · Fernando Calamante[5] · Amit Mehndiratta[1,6]

Abstract

Objective To implement an advanced spatial penalty-based reconstruction to constrain the intravoxel incoherent motion (IVIM)–diffusion kurtosis imaging (DKI) model and investigate whether it provides a suitable alternative at 1.5 T to the traditional IVIM–DKI model at 3 T for clinical characterization of prostate cancer (PCa) and benign prostatic hyperplasia (BPH).

Materials and methods Thirty-two patients with biopsy-proven PCa were recruited for MRI examination ($n = 16$ scanned at 1.5 T, $n = 16$ scanned at 3 T). Diffusion-weighted imaging (DWI) with 13 b values (b = 0 to 2000 s/mm^2 up to 3 averages, 1.5 T: TR = 5.774 s, TE = 81 ms and 3 T: TR = 4.899 s, TE = 100 ms), T2-weighted, and T1-weighted imaging were used on the 1.5 T and 3 T MRI scanner, respectively. The IVIM–DKI signal was modeled using the traditional IVIM–DKI model and a novel model in which the total variation (TV) penalty function was combined with the traditional model to optimize non-physiological variations. Paired and unpaired t-tests were used to compare intra-scanner and scanner group differences in IVIM–DKI parameters obtained using the novel and the traditional models. Analysis of variance with post hoc test and receiver operating characteristic (ROC) curve analysis were used to assess the ability of parameters obtained using the novel model (at 1.5 T) and the traditional model (at 3 T) to characterize prostate lesions.

Results IVIM–DKI modeled using novel model with TV spatial penalty function at 1.5 T, produced parameter maps with 50–78% lower coefficient of variation (CV) than traditional model at 3 T. Novel model estimated higher D with lower D^*, f and k values at both field strengths compared to traditional model. For scanner differences, the novel model at 1.5 T estimated lower D^* and f values as compared to traditional model at 3 T. At 1.5 T, D and f values were significantly lower with k values significantly higher in tumor than BPH and healthy tissue. D (AUC: 0.98), f (AUC: 0.82), and k (AUC: 0.91) parameters estimated using novel model showed high diagnostic performance in cancer lesion detection at 1.5 T.

Discussion In comparison with the IVIM–DKI model at 3 T, IVIM–DKI signal modeled with the TV penalty function at 1.5 T showed lower estimation errors. The proposed novel model can be utilized for improved detection of prostate lesions.

Keywords Intravoxel incoherent motion · Diffusion kurtosis imaging · Prostate cancer · Benign prostatic hyperplasia · Total variation penalty function

✉ Amit Mehndiratta
amit.mehndiratta@keble.oxon.org

1 Centre for Biomedical Engineering, Indian Institute of Technology Delhi, Hauz Khas, New Delhi 110016, India

2 Department of Radio-Diagnosis, All India Institute of Medical Sciences, New Delhi, India

3 Department of Nuclear Magnetic Resonance, All India Institute of Medical Sciences, New Delhi, India

4 Department of Physics, Indian Institute of Technology Delhi, New Delhi, India

5 Sydney Imaging and School of Biomedical Engineering, University of Sydney, Sydney, Australia

6 Department of Biomedical Engineering, All India Institute of Medical Sciences, New Delhi, India

Introduction

Prostate cancer (PCa) and benign prostatic hyperplasia (BPH) are the two most common diseases of prostate gland. Serum prostate-specific antigen (PSA) test and digital rectal examination (DRE) are used for screening of PCa [1]. Patients with elevated PSA levels (> 4 ng/mL) and/or abnormal findings on DRE are advised to undergo transrectal ultrasound (TRUS) guided biopsy of prostate for diagnosis of PCa [2]. However, it has a low specificity for localization and characterization of small lesions and might cause bleeding and inflammation in patients [3]. In contrast, MRI-guided biopsies have shown potential in detecting missed regions of cancer from previous negative biopsies and persistent cancer concerns. Thus, it is currently the recommended procedure wherever possible [3, 4].

Current clinical standards follow a combination of systemic and targeted biopsy with a higher detection rate for prostate lesions [4]. In targeted biopsy, multi-parametric MRI (mp-MRI) is now widely accepted for the prostate lesion localization and characterization with an improved specificity [5]. Diffusion-weighted imaging (DWI) is a non-invasive imaging method that measures microscopic transitional motion of water molecules in extracellular space. DWI can be quantified by monoexponential model (ME) using gradient b-factor > 200 s/mm^2 based on free water diffusion to quantify the apparent diffusion coefficient (ADC). Cancerous lesions commonly manifest with a higher water restriction, i.e., lower ADC value, associated with an uncontrolled cell growth; commonly observed in PCa also [6, 7]. However, water diffusion around tumor tissue deviates from this simplified model assumption because water is restricted due to densely packed tumor tissues and thus, ADC fails to fully capture the intravoxel diffusion heterogeneity of tumor [8]. Therefore, a different comparative model proposed kurtosis imaging with high b values that might capture this variability and is also been evaluated in prostate cancer imaging in the past [9, 10]. Advanced DWI approaches take this issue further into account by acquiring multi b-values (e.g., from 0 to 2000 s/mm^2) and analyzing the signal using the intravoxel incoherent motion (IVIM) and diffusion kurtosis imaging (DKI). Le Bihan et al. [11] introduced IVIM methodology, modeling both the diffusion and perfusion components together, providing a quantitative information on microstructural and microvasculature distinctly. It is worth noting that both ADC and IVIM models consider an underlying free water diffusion with an Gaussian distribution assumption. Whereas DKI methodology developed by Jensen et al. [12] assumed that water movement is a non-Gaussian distribution due to complex structure of the tissues and its pathophysiological variations; providing a realistic variation to capture the tissue heterogeneity.

Lu et al. 2012 modeled IVIM and DKI simultaneously as a hybrid model, to estimate both diffusion and perfusion parameters from IVIM model, and k parameter from DKI model [13]. The hybrid IVIM–DKI model more accurately captured the complexity of tumor microstructure compared to the conventional monoexponential, IVIM, or DKI model alone [13, 14]. However, this hybrid model suffered from local non-physiological heterogeneity in parameter estimation due to low SNR of the data [13]. This analysis can be further improved using a constrained parameter reconstruction approach, such as total variation (TV) penalty function [15]. This regularization approach provides an adaptive spatial homogeneity by removing spurious values that may arise during parametric reconstruction of the image [15, 16]. TV penalty function has been successfully implemented for IVIM analysis, and studies have shown its robustness in different cancers, e.g., bone tumor [16, 17], PCa [18] and lymphoma [19]. These studies used TV reconstruction on 2D parameter maps. The quantitative improvement that this methodology can offer with implementation of 3D TV reconstruction for IVIM–DKI hybrid model and its clinical use at different magnetic strengths are the research questions for the current study. Also, there has been a clear trend to shift from mp-MRI (with contrast injection) to biparametric MRI (bp-MRI without contrast injection) for clinical applications, because of inherent issues related to the use of contrast agents [5]. Hence, this study intended to explore the utility of IVIM–DKI in prostate cancer lesion detection, as it can provide microvascular perfusion information without using exogenous contrast agent.

Most used MR scanners in clinical routine have magnetic field strengths of 1.5 T and 3 T. The latter provides a higher signal-to-noise ratio (SNR), thus often preferred by radiologists [4]. However, 3 T MRI suffers from artifact due to tissue susceptibility and signal heterogeneity [4]. In remote regional areas (i.e., areas not close to major cities) and developing countries more broadly, there is also limited availability and accessibility to these high-field MRI [20]. Therefore, the benefits of such a field strength are not readily available. To address these deficiencies, one of the objectives of this study includes implementing a novel TV penalty function-based reconstruction to stabilize the solution of the traditional IVIM–DKI model. Given that most IVIM–DKI studies have been carried out exploiting the benefits provided by 3 T MRI [21–24]. This study also investigates whether the use of such an advanced reconstruction approach at 1.5 T makes it a suitable alternative to the traditional IVIM–DKI model at 3 T and assesses their role in detecting prostate lesions, i.e., prostate cancer and benign prostatic hyperplasia.

Materials and methods

Subjects and clinical data acquisition

Approval from the Institutional review board was obtained; all patients were enrolled only after their written informed consent. Age-matched total thirty-two male patients ($n = 32$) with biopsy-proven PCa were recruited, as shown in Table 1. After six weeks from biopsy, sixteen patients ($n = 16$) were scanned using 1.5 T MRI (Achieva; Philips Healthcare, Best, the Netherlands) and sixteen patients ($n = 16$) were scanned 3 T MRI (Ingenia; Philips Healthcare, Best, the Netherlands) in a period from January 2018 to November 2019. Table 1 also shows no significant difference ($p > 0.05$) in the two cohorts recruited under two MRI machines.

Conventional MR protocol including T2-weighted, T1-weighted and DWI were acquired for all the patients. IVIM–DKI was acquired using 13 b-factors b value = 0, 25, 50, 75, 100, 150, 200, 500, 800, 1000, 1250, 1500, 2000 s/mm^2) with three diffusion-encoding gradient directions (gradient overplus option enabled) up to three averages. The number of b values was chosen based on the current recommendations [25] and was consistent with the published clinical studies in prostate [7, 26, 27]. IVIM–DKI data were acquired using a 32-channel phased-array surface coil for both MR system; using multi-slice Spin Echo (SE) with axial single-shot echo planar imaging (EPI) with FOV = 240×240 mm^2; Acquisition matrix: 108×110; Reconstruction matrix 240×240; acquisition voxel: $2.22 \times 2.22 \times 4$ mm^3, interpolated to $1 \times 1 \times 4$ mm^3 with no slice gap; number of signals averaged = 3; 1.5 T: TR = 5.774 s, TE = 81 ms with DELTA/delta = 42/28.9 ms and diffusion time = 32.4 ms; 3 T: TR = 4.899 s, TE = 100 ms with DELTA/delta = 50/24.9 ms

and diffusion time = 41.7 ms; fat suppressed using spectral presaturation with inversion recovery (SPIR). For 1.5 T, half scan was enabled with factor 0.69; whereas, for 3 T half scan was disabled and multiple TE (delta TE) were not used for both the MR system. T2-weighted images were used to identify patients with excessive rectal gas. Total of 12 patients (1.5 T: 5 patients and 3 T: 7 patients) were inserted with an infant feeding tube per rectum lubricated with lignocaine jelly to remove the gas before further MRI acquisition to avoid any EPI-DWI-related artifacts.

Quantitative image analysis

All parameters were estimated using non-linear least-square optimization and parallel computing with an in-house built toolbox for diffusion MRI analysis using MATLAB (version 9.1, The MathWorks, Inc., Natick, MA, USA). ADC was calculated voxelwise using ME model using three b values = 0, 500, and 1000 s/mm^2, defined in Eq. 1:

$$\frac{S}{S_0} = e^{-b\text{ADC}} \tag{1}$$

Four parameters define the IVIM–DKI model, where D is free water diffusion coefficient, D^* is pseudo-diffusion coefficient representing micro-circulations of the capillary networks, f is perfusion fraction, and k is kurtosis. IVIM–DKI parameter estimation was performed using all the 13 b values (0–2000s/mm^2) and two methods (i) Hybrid model ('hybrid' in the sense that integrating non-Gaussian DKI model with the IVIM model, which will be referred to as 'traditional' model)[13] as shown in Eq. 2:

$$\frac{S}{S_0} = fe^{-bD^*} + (1-f)e^{-bD + \frac{1}{6}(bD)^2 k} \tag{2}$$

where S and S_0 are diffusion signals with and without diffusion gradient b in s/mm^2. Initial values used optimization routine of traditional model [7, 9, 26, 28] and further details are available in the supplementary materials; and (ii) Hybrid model with TV (referred to as 'novel' model, from now on). The novel model was implemented using the same model as in Eq. 2 with TV penalty function in-built into the optimization routine, which resulted in parameter map that possessed spatial homogeneity [16]. Novel model is a constrained minimization problem in which, any sudden change in parameter estimation due to least-square optimization is balanced out by the corresponding parameter due to the reduction in TV penalty function iteratively [16]; as shown in Eq. 3:

$$\min_X f(X) = \min_X [||X - X'||^2 + \alpha \text{TV}(X)] \tag{3}$$

where X and X' are expected and observed images (of size $M \times N \times S$), α is a weight parameter between the two cost functions, and TV(X) penalty of 3D parameter map is the L1

Table 1 Clinical, pathological and radiological characteristics of PCa patients

Clinical characteristics	1.5 T	3 T	p value
No. of patients	16	16	–
Age (years) (mean ± SD)	61.94 ± 5.47	66.19 ± 6.85	$p > 0.05$
Gleason grade			$p > 0.05$
3 + 3	9	7	
3 + 4	0	4	
4 + 3	3	0	
4 + 4	0	3	
4 + 5	3	2	
5 + 4	1	0	
PIRAD score			$p > 0.05$
3	1	0	
4	6	6	
5	9	10	

norm of discrete image gradient as shown in Eq. 4. Advantage of 3D TV is that it also considers neighboring voxels in the transverse direction and reconstructs the whole 3D dataset [29]. Image gradient (as shown in Eq. 4) is calculated by updating the parameter values under every iteration:

$$TV(X) = \sum_{i,j,k=1}^{M,N,S} \sqrt{(R_x X)^2 + (R_y X)^2 + (R_z X)^2} \qquad (4)$$

where X, is the parameter value at voxel (i:1, 2, 3…, M; j:1, 2, 3…, N; k:1, 2, 3, …, S) and $R_x X = X_{(i,j,k)} - X_{(i+1,j,k)}$, $R_y X = X_{(i,j,k)} - X_{(i,j+1,k)}$, and $R_z X = X_{(i,j,k)} - X_{(i,j,k+1)}$. The IVIM–DKI with TV algorithm is available upon request, and is also available by open access at (https://github.com/amitvmehndiratta/IVIM-DKI-MRMP2021).

Data fitting quality of both traditional and novel models was evaluated using correlation coefficient, which was more than 0.96 for novel model in each tissue types (tumor, healthy PZ, and BPH). These results were consistent with the results from the implementation of TV for IVIM model proposed earlier by Baidya Kayal et al. [16]. Traditional and novel model voxel-level fitting were compared to raw IVIM–DKI signal in a voxel for each ROI; details are shown in the supplementary material (Supplementary Figures S1.1–S1.10).

SNR was estimated for the trace DWI image at $b=0$ s/mm^2 and 1000 s/mm^2 by taking the ratio of the mean signal value of the ROI (healthy PZ, tumor, and BPH) to 1.53 times the standard deviation (SD) of the signal value in the background, where background ROI for every patient was drawn outside of body [30].

ROI localization

All ROIs were drawn manually using the MRICron software (http://www.cabiatl.com/mricro/mricron/index.html). All the enrolled patients had at least one or more biopsy-proven lesions. Two experts CJD and AN drew the lesion ROIs, having more than ten years and three years of experience, respectively, in prostate MR imaging. Among all 32 subjects enrolled, two patients had no BPH nodules, and one patient did not show any healthy region in the prostate for ROI selection. Multiple lesions were found in patients with high-grade PCa; thus, only biopsy-proven positive lesions were selected for tumor ROI marking. Lesions with hyperintense in DWI at $b=2000$ s/mm^2 and hypointense in ADC map were the characteristics used to localize tumor and define the tumor ROI. T2-weighted images were used to check tumor (hypointense region) present in the transitional zone. ROI for BPH lesion was chosen using $b=0$ s/mm^2 and T2-weighted image: BPH ROI was drawn on $b=0$ s/mm^2 image, with reference to hypointense or hyperintense region in the corresponding region in T2-weighted image. Healthy area of prostate was chosen in the peripheral zone (PZ) only. Healthy PZ ROI was drawn in similar location for all patients, and healthy PZ ROIs did not include any part of the tumor or BPH and were confirmed using DWI at $b=2000$ s/mm^2 and ADC map. Shape of tumor ROI for all cases was different to accommodate the individual tumor shape. Number of voxels in tumor ROIs was compared with number of voxels in BPH and healthy PZ ROIs to approximately match the ROI sizes (~80–140 voxels) with tumor ROI in every patient. Examples of tumor ROI (158 ± 104 voxels), Healthy PZ (140 ± 90 voxels), and BPH (78 ± 48 voxels) ROI are illustrated in Fig. 1 for a representative patient.

Statistical tests

Precision of parameter maps was estimated using coefficient of variation (CV (%), as ratio of standard deviation to the mean value × 100) for each individual parameter, where lower CV indicated a good precision. Combined CV (CV$_{comb}$) for a method was calculated by averaging the individual CV for all the four parameters of IVIM–DKI.
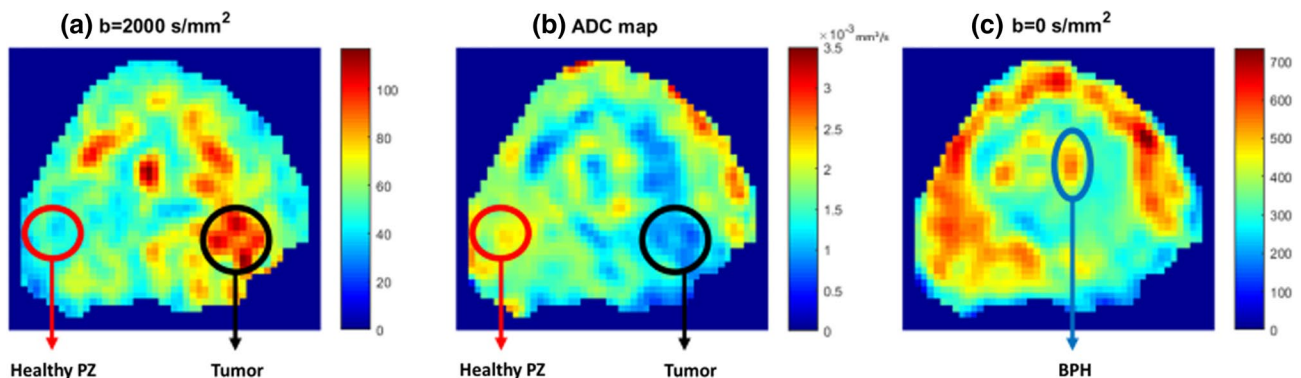

Fig. 1 ROI localization of tumor (black circle), healthy PZ (red circle) and BPH (blue circle) using IVIM–DKI at (**a**) $b=2000$ s/mm^2, (**b**) ADC map, and (**c**) $b=0$ s/mm^2 for one representative patient (65 years old) having *p*rostate cancer with Gleason score of 7 (4+3) acquired at 1.5 T

Within-scanner agreement between parameters evaluated using novel model and traditional model was assessed using paired *t*-tests. Unequal variance *t*-test (unpaired with two-tail assumption) was used to compare significant (p value < 0.05) differences between the group measurements at 1.5 T and 3 T (i.e., between-scanner group differences).

Fitting quality of traditional and novel model was calculated for all ROIs using AIC (Akaike Information Criterion) and AICc (AIC corrected)[31].

One-way ANOVA with Tukey's multiple comparison test was used to compute significant differences (p value < 0.05) between IVIM-DKI parameter values among healthy PZ, tumor, and BPH.

Diagnostic performances of novel model at 1.5 T and traditional model at 3 T were assessed using receiver operating characteristics (ROC) analysis regression model with cut-off values, area under the ROC curve (AUC), sensitivity, and specificity (using MedCalc, version 19.1.7, MedCalc Software, Ostend, Belgium).

Results

Within-scanner performance comparison between traditional and novel model for IVIM–DKI parameter estimation

Parameter estimation using novel model was compared with traditional model to evaluate agreement between both models at 1.5 T. Overall, there were significant differences (p value < 0.05) between traditional and novel models for all IVIM–DKI parameters. D parameter calculated using novel model was higher (p value < 0.001) than estimated using the traditional model (Fig. 2b). D^*, f, and k parameters estimated using novel model were lower (p value < 0.05) than the parameters calculated using traditional model (Fig. 2c–e). Same trend was also observed for parameter estimation at 3 T, where parameters estimated by novel model were significantly (p value < 0.05) higher for D and lower for D^*, f, and k than the traditional model, presented in Fig. 2b–e. It indicates that the novel model with total variation function shows a consistent difference in parameter values across both the field strengths.

For all three tissue types, parameter estimated using traditional and novel model were considerably different (p value < 0.05) D was higher and D^*, f, and k lower for novel model than the traditional model, except for k parameter in healthy PZ (at 3 T) and tumor ROI as shown in Fig. 2.

In comparing the precision of the parameter estimation at 1.5 T, novel model showed significantly (p value < 0.01) lower CV_{comb} by factor of 63–73% than the traditional model. Also, a similar improvement (as measured by 54–67% decrease in CV_{comb}) in parameter estimation by
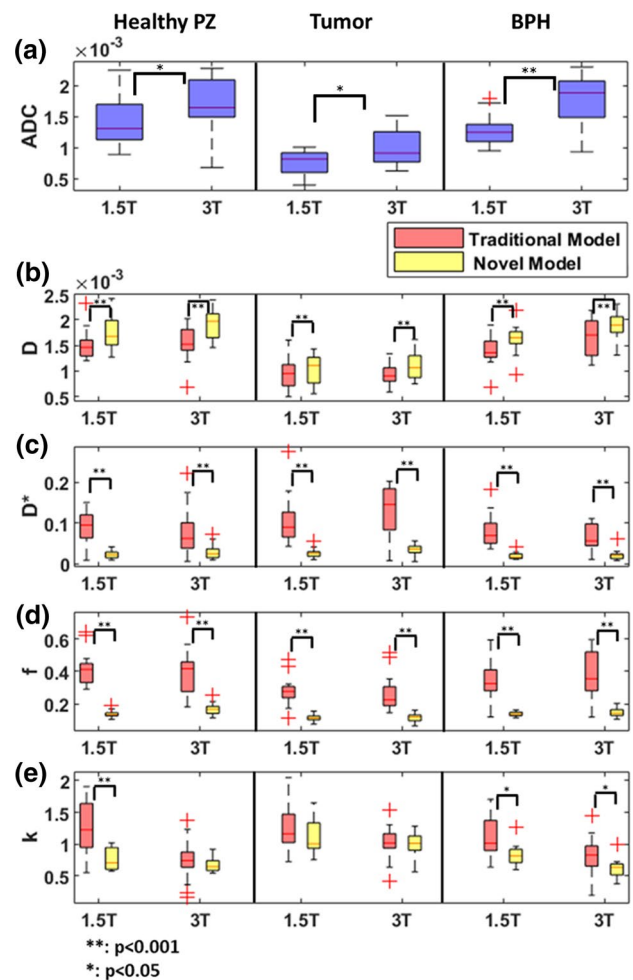

Fig. 2 Box-whisker plot showing (**a**) ADC and comparison between novel (yellow) and traditional model (red) estimated parameters (**b**) D, (**c**) D^*, (**d**) f, and (**e**) k for healthy PZ, tumor, and BPH ROI using IVIM–DKI image at 1.5 T and 3 T

novel model was observed over traditional model at 3 T, suggesting the improvement with TV is consistent across both the field strengths, as shown in Fig. 3.

For all the tissue types, lower CV_{comb} was observed for novel model (healthy PZ: lower by 57–63%, tumor: lower by 54–63%, and BPH: lower by 67–73%) than the traditional model at both the field strengthens, as presented in Fig. 3.

The fitting quality of traditional and novel model was analyzed using AIC and AICc individually at both field strengths, 1.5 T and 3.0 T. For traditional model, AIC and AICc ranged -23.2 to -22.9 and -14.7 to -14.3, respectively. For novel model AIC and AICc were ranged -22.8 to -23 and -14.6 to -14.2, respectively, at 1.5 T. Similar trends were also observed at 3 T MRI, where for traditional model, AIC and AICc ranged from -22.9 to -22.8 and -14.3 to -14.2, respectively and for novel model, AIC and AICc values varied from -22.8 to -22.5 and -14.2 to -13.9, respectively. These results indicate that the fitting
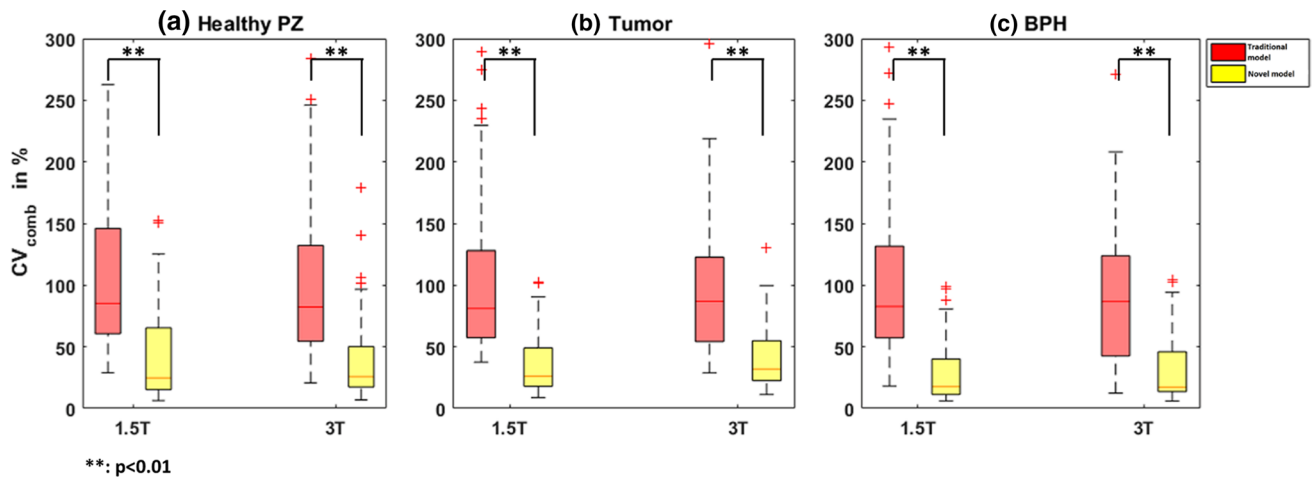
Fig. 3 Box-whisker plot showing CV_{comb} for (**a**) healthy PZ, (**b**) tumor, and (**c**) BPH ROIs, calculated for traditional (red) and novel (yellow) model using IVIM–DKI image from 1.5 to 3 T

quality (in-terms of AIC and AICc) of traditional and novel model was similar. However, novel model has significantly lower CV ($p < 0.05$) than the traditional model leading to less spurious values in the parametric reconstruction.

Performance comparison between traditional model at 3 T and novel model at 1.5 T for IVIM–DKI parameter estimation

TV-based parametric reconstruction (i.e., novel model) at low-field strength (1.5 T) was compared with the traditional model parametric reconstruction at high-field strength (3 T). For $D*$ and f parameters, significant differences (p value < 0.001) were observed between novel model at 1.5 T and traditional model at 3 T. Interestingly, variation in parameter estimations using novel model at 1.5 T was still lower than the traditional model at 3 T for $D*$ and f, as shown in Fig. 2c, d. ADC measurements using traditional

monoexponential model were also significantly different (p value < 0.05) at 1.5 T and 3 T, as shown in Fig. 2a.

For all three tissue types, IVIM–DKI parameters estimated using novel model at 1.5 T were significantly lower (p value < 0.001) than the estimations obtained from traditional model at 3 T; with voxel-wise variance in ROI lower by factor of 2–3 times in novel model than the traditional model. Similarly, an improved precision producing 54–68% lower CV_{comb} was observed for the novel model at 1.5 T (p value < 0.01) than the traditional model at 3 T, as shown in Table 2.

Even in parameter-wise comparison among three tissues, novel model at 1.5 T showed significantly (p value < 0.01) lower CV than traditional model at 3 T. For healthy PZ, novel model at 1.5 T showed lower CV (CV_D: 58%, CV_{D*}: 24%, CV_f: 52%, and CV_k: 82%) than traditional model at 3 T, respectively, as shown in Table 2. Similar trends were observed in tumor (CV_D: 50%, CV_{D*}: 51%, CV_f: 61%, and

Table 2 Coefficient of variation (CV (%)) of D, $D*$, f, and k in healthy PZ, tumor and BPH obtained from IVIM–DKI parameter estimation using novel model at 1.5 T and traditional model at 3 T

IVIM–DKI PARAMETER	Healthy PZ		Tumor		BPH	
	Traditional model (at 3 T)	Novel (at 1.5 T)	Traditional model (at 3 T)	Novel (at 1.5 T)	Traditional model (at 3 T)	Novel (at 1.5 T)
D	42 ± 19	$16 \pm 8^{\dagger}$	42 ± 11	$20 \pm 6^{\dagger}$	34 ± 11	$12 \pm 4^{\dagger}$
$D*$	179 ± 81	$102 \pm 26^{\dagger}$	175 ± 112	$74 \pm 17^{\dagger}$	189 ± 72	$68 \pm 16^{\dagger}$
f	79 ± 27	$32 \pm 14^{\dagger}$	96 ± 22	$35 \pm 10^{\dagger}$	79 ± 24	$21 \pm 9^{\dagger}$
k	114 ± 43	$18 \pm 8^{\dagger}$	86 ± 36	$17 \pm 7^{\dagger}$	108 ± 65	$15 \pm 7^{\dagger}$
CV_{comb}	103 ± 59	42 ± 40	100 ± 56	37 ± 26	103 ± 65	29 ± 27

Data values are represented as mean ± SD (standard deviation)

D diffusion coefficient, $D*$ pseudo-diffusion coefficient, f perfusion fraction, k kurtosis, CV_{comb} coefficient of Variation combined

†Significant differences between traditional and novel model with p value < 0.01

CV_k: 78%) and BPH (CV_D: 62%, CV_{D*}:57%, CV_f: 70%, and CV_k: 82%) regions with low CV using novel model at 1.5 T than the traditional model at 3 T.

Qualitative and quantitative comparison of parameter estimation at 1.5 T and 3 T

Figure 4 shows IVIM–DKI parameter reconstruction for two representative patients with PCa having PIRADS-v2 score of 4, where one patient dataset was acquired at 1.5 T (Fig. 4a) and the other at 3 T (Fig. 4b). Results for ten more patients are presented in the Supplementary material Figures S1.1–S1.10. Qualitatively, parameter maps evaluated

using novel model appeared smooth, whereas traditional model produced maps showing spurious high values and low quality at both field strengths. Tumor in both 1.5 T and 3 T seemed consistent hypointense in D and f map, whereas it appeared hyperintense in $D*$ and k maps. Corresponding tumor region in T2-weighted image section also showed hyperintense region and photomicrograph of radical prostatectomy specimen showed viable prostatic acinar adenocarcinoma, Gleason grade, 3+3, grade group 1 in both patients Fig. 4a, b.

Figure 5 shows box-whisker plot for ADC and all four IVIM–DKI parameters evaluated using (a) novel model at 1.5 T and (b) traditional model at 3 T. Differentiation
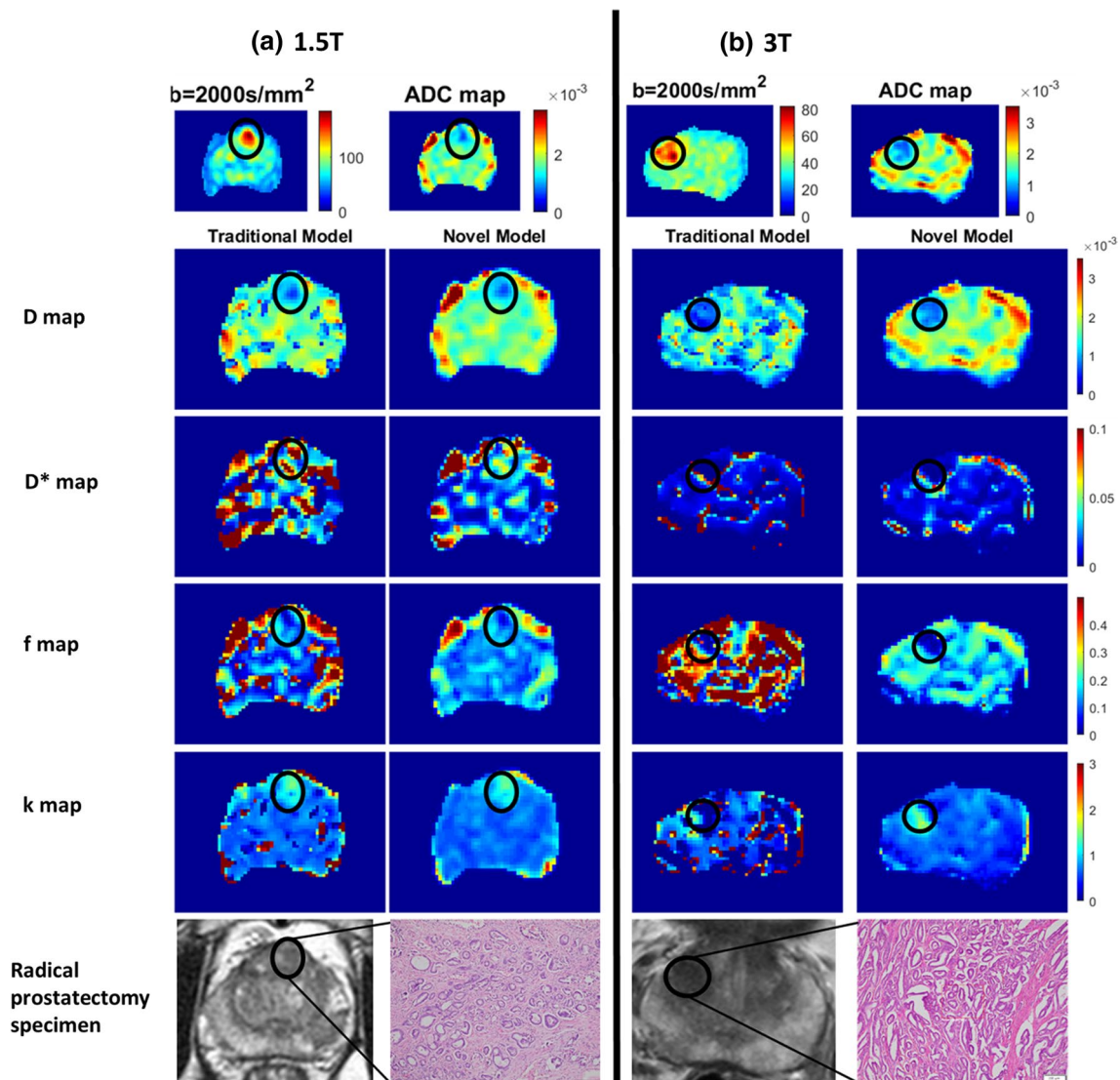

Fig. 4 IVIM–DKI parameter maps of representative patients (**a**) male, 61 years and (**b**) male, 60 years) with PIRADS 4 lesion encircled by black circle. Tumor appearing hypointense on D and f map and hyperintense on $D*$ and k map obtained from traditional and novel models at (**a**) 1.5 T and (**b**) 3 T. Section of T2-weighted image shows hyperintensity in the region of tumor and photomicrograph of radical prostatectomy specimen showing prostatic acinar adenocarcinoma, Gleason grade, 3+3, grade group 1 in both patients (**a**) and (**b**). Parameter maps obtained from novel model are reasonably less noisy than parameter maps from traditional model
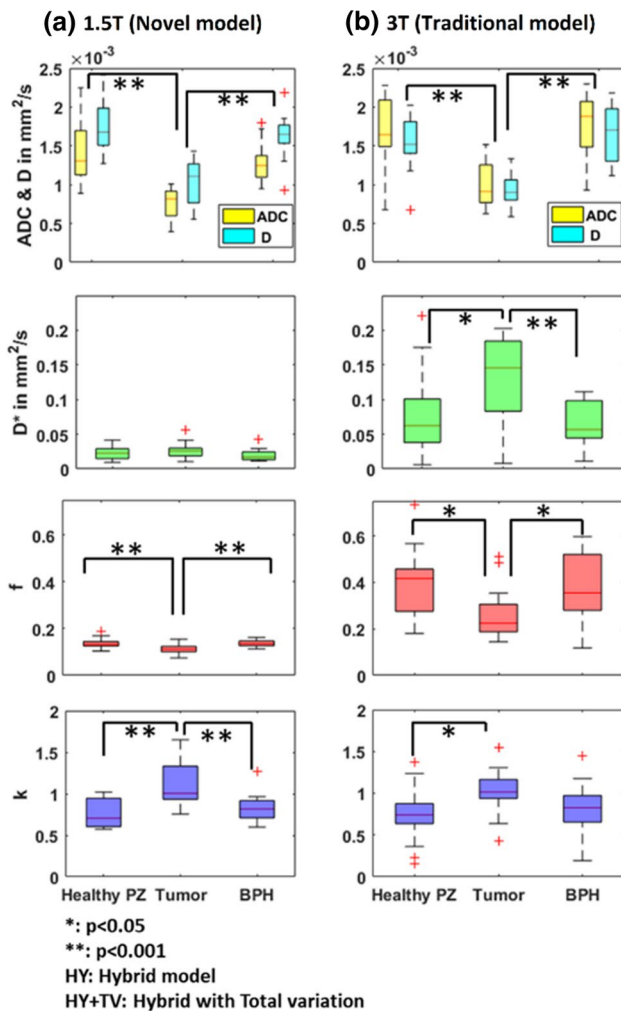
Fig. 5 Box-whisker plot of ADC and IVIM–DKI parameters (*D*, *D**, *f*, *k*) in healthy PZ, tumor and BPH evaluated using (**a**) novel model at 1.5 T and (**b**) traditional model at 3 T

In comparison, higher value of *k* was observed for tumors as compared to healthy PZ (p value < 0.01) and BPH (p value < 0.01). Parameter *D** no significant differences were observed between tumor against healthy PZ and BPH.

Similar trend was observed for the traditional model at 3 T, differentiation between healthy PZ, tumor and BPH were observed with lower ADC (p value < 0.01), *D* (p value < 0.01), and *f* (p value < 0.05) in tumor as compared to healthy PZ and BPH. A higher value of *k* was observed for tumors than healthy PZ (p value < 0.05). *D** was observed higher for tumors against healthy PZ (p value < 0.05) and BPH (p value < 0.01). Also, worth noting that traditional model have shown high variability in parameter estimation for *D** and *f* than the novel model.

Diagnostic performance of IVIM–DKI parameters using novel model at 1.5 T and traditional model at 3 T in PCa detection

The highest AUC was observed for *D* parameter with 0.98 (0.86–1) for the novel model at 1.5 T (with cut-off values 1.4×10^{-3} mm²/s, sensitivity: 94% and specificity: 94%). Whereas *f* (AUC = 0.82 (0.64–0.93)) and *k* (AUC = 0.91 (0.76–0.98)) parameter using novel model at 1.5 T also showed higher AUC as compared to traditional model at 3 T (*f*: AUC = 0.76 (0.57–0.89) and *k*: AUC = 0.75 (0.56–0.88)). Overall results for traditional model at 3 T showed lower AUC than novel model at 1.5 T, except for *D** parameter, as shown in Table 3.

Discussion

IVIM–DKI is a unique analysis methodology that can simultaneously and noninvasively measure diffusion and perfusion characteristics of the tissue with an assumption of non-Gaussian distribution of the underlying water movement in the tissues. This study is the first to compare parameter reconstruction of IVIM–DKI model for datasets acquired at

between healthy PZ, tumor, and BPH using novel model at 1.5 T showed lower ADC, *D*, and *f* in tumor as compared to healthy PZ (p value < 0.01) and BPH (p value < 0.01).

Table 3 Diagnostic performance of IVIM–DKI parameters obtained from novel model at 1.5 T and traditional model at 3 T in PCa detection

IVIM–DKI parameters	AUC		Cut off		Sensitivity %		Specificity %	
	1.5 T (Novel model)	3 T (Traditional model)	1.5 T (Novel model)	3 T (Traditional model)	1.5 T (Novel model)	3 T (Traditional model)	1.5 T (Novel model)	3 T (Traditional model)
D†	0.98 (0.86–1)	0.92 (0.8–0.99)	1.4	1.1	94	88	94	93
*D**†	0.63 (0.44–0.79)	0.75 (0.56–0.89)	23.3	73.6	63	88	69	67
f	0.82 (0.64–0.93)	0.76 (0.57–0.89)	0.2	0.4	63	88	94	67
k	0.91 (0.76–0.98)	0.75 (0.56–0.88)	0.7	0.9	100	75	69	80

Data in parenthesis consist of 95% confidence interval

D diffusion coefficient, *D** pseudo-diffusion coefficient, *f* perfusion fraction, *k* kurtosis

two different field strengths, 1.5 T and 3.0 T, to the best of our knowledge. IVIM–DKI datasets were analyzed using traditional hybrid model producing parametric maps, which were susceptible to noise and had non-physiological heterogeneity at both field strength. The study demonstrated that even with the lower magnetic strength (at 1.5 T), which is widely available clinically, the novel model based IVIM–DKI reconstruction outperformed the traditional model both qualitatively and quantitatively with lower variance and CV and having a higher diagnostic performance. These observations imply that incorporating TV constrain into traditional model can help to estimate clinically useful IVIM–DKI maps even with lower field strength, and therefore extend the reliability of IVIM–DKI at a field strength more widely accessible in some countries and regional settings.

Recent studies have shown indistinguishable differences between ADC values from 1.5 T to 3 T [32, 33]; also both being reliable for PCa detection [34, 35]. Even prostate imaging reporting and data system (PIRADS) scoring, which is radiologically used to evaluate PCa for multi-parametric MRI, does not consider the quality of MRI data as acquired at 1.5 T or 3 T [35] or even the parameter reconstruction quality. Although 3 T provides higher SNR and expected to have a better resolution in DWI, it also suffers from few limitations, such as susceptibility distortions and chemical shift artifacts [36]. In this study, SNR of trace DWI image at $b = 0$ s/mm^2 and 1000 s/mm^2 was about 17 and 9, respectively, at 1.5 T; whereas for 3 T, SNR of trace DWI image at $b = 0$ s/mm^2 and 1000 s/mm^2 was approximately 28 and 18, respectively. Also, there were no cases with severe susceptibility artifacts or geometric distortions in any trace DWI images. Representative images of trace DWI of the four patients are presented in supplementary material Figure S2–S5. In terms of accessibility and affordability of 3 T scanner, it is essential to recognize that it has been challenging in remote regional areas globally, especially in developing countries [37].

An optimal solution for this issue would be through reliable imaging analysis methods using existing 1.5 T MRI scanners, with improved image quality using better parametric reconstruction methods. The traditional model for IVIM–DKI considers voxel as independent entities, resulting in non-physiological heterogeneity in the resulting parameter maps. In contrast, in this study, a novel parameter reconstruction method for IVIM–DKI method was implemented using TV as a regularization function. The goal was to simultaneously model all the voxels containing IVIM–DKI signal using the traditional model with a spatial TV penalty function. There was no requirement of tuning or manual intervention for the novel model as it adaptively corrects spatial inhomogeneities by removing any abrupt changes. TV correlates between neighboring voxels that are spatially related along with in all planes for 3D parameter map reconstruction [29] and at the same time, it is known to have an edge-preserving regularization character. This model's adaptive nature allows one to select a suitable solution, such that the solution possesses the spatial homogeneity property. Thus, TV constraint prevents the solution from getting stuck in undesirable local minima by iteratively updating the initial values and still preserving heterogeneity among different tissue types.

Recent previous studies have shown that TV penalty function was successful in addressing these issues with the IVIM model (which accurately estimated parameters with low noise both in simulations and clinical datasets such as osteosarcomas [16, 17], Ewing sarcoma [16], PCa [18], and lymphoma [19]). Importantly, it had been already shown earlier by Lu et al. [13] that IVIM–DKI accurately models the signal decay of tumor tissue voxels compared to any other models such as monoexponential, DKI, and biexponential models, as tumor possess high heterogeneity [13]. Therefore, to evaluate both diffusion and perfusion, IVIM–DKI model was the natural choice for our study to consider. It simultaneously models diffusion and perfusion while also incorporating tissue heterogeneity through kurtosis. Machine learning-based IVIM analysis was not possible with the limited data, as machine learning algorithms rely upon a more extensive training set. However, a simpler reconstruction technique with the spatial regularized method proposed in this study can circumvent this challenge as it can still work well even with limited data and without relying on training of large sample and computational expense.

In the current study, agreement and precision between parameter estimation by traditional and novel models at 1.5 T and 3 T field strength were analyzed to evaluate differences between parameter estimates produced by both models and coefficient of variation. Irrespective of MR-field strength used, overall, novel model showed quantitatively better reconstruction and lower variation in estimation of parameters than the traditional model. This is certainly related to TV's effectiveness in reducing abrupt variations in parameter values due to its improved noise reducing performance (same as supported by [16–18]). Also, estimation using novel model produced lower CV_{comb}, with highest reduction in CV (lower 24–82%) in prostate lesion at both field strengths. However, it should be noted that no conclusion can be made about increased accuracy, given the lack of ground-truth information for these parameters. Traditional and novel models showed similar AIC and AICc for all ROIs; however, novel model produced less error with low CV and better-quality parameter maps.

This study also sought to evaluate the quantitative characteristics of IVIM–DKI parameter maps reconstructed with novel model at 1.5 T (lower field strength) compared to parameters calculated using traditional model at 3 T

(higher field strength). D^* and f parameters estimated using novel model at 1.5 T showed smaller CV and were significantly different than the parameters estimated using traditional model at 3 T; once again due to the TV algorithm, which reduces noise while performing parameter estimation using novel model. Consistently all the parameters (D, D^*, f, and k) calculated with the novel model at 1.5 T showed lower CV values (by 50–82%) against traditional model at 3 T in all three tissue types. The CV for D^* was higher for all three tissue types than the other three parameters (D, f, k) irrespective of MR strength used, which indicated a qualitatively inferior image of D^*, suggesting possibly limited usefulness of the parameter for clinical interpretation currently. Also, ADC estimated at 1.5 T was quantitatively different from 3 T with CV about 19–28%. Previous studies using phantoms have suggested that ADC measurements might differ across field strength and absolute values may vary, which warrants further investigations [38, 39].

Qualitatively, hypointensity with spatial homogeneity was observed in tumor region for D and f parameter maps with the novel model at 1.5 T. Similarly, k parameter map showed hyperintense with homogeneity in tumor region. D^* showed high CV calculated from both models, and thus it becomes difficult to interpret the clinical use of it. Regardless of MR-field strength used, the novel model can still successfully reduce the non-physiological heterogeneity in IVIM–DKI parameter maps.

For both MR systems, tumor showed significantly lower ADC than healthy tissue and BPH; however, ADC is affected by water diffusion and perfusion around tumor region. Also, in recent literature, ADC showed a better accuracy for differentiating tumors vs. BPH, whereas IVIM parameters were not shown to capture the crucial differences [7, 9, 28]. In this study, IVIM–DKI parameters in tumor region showed better interpretation, such as D and f were significantly lower than healthy tissue and BPH at both the field strengths. The k parameter was significantly higher in tumors than healthy tissue and BPH with novel model at 1.5 T. In contrast, for traditional model with 3 T, k showed difference only among tumor and healthy PZ with no difference from BPH. Causation of low D values in tumor region is likely related to poor cell differentiation with densely packed epithelial cells, restricting water movement [6]. Also, low f and high k in the tumor region suggested that there might be poor vasculature and increased tissue heterogeneity [40]. In contrast, BPH showed high D and low k compared to PCa, mainly of stromal or glandular nodules with smooth muscles surrounding it. D^* values estimated using traditional model at 3 T were observed to be consistently higher than the values estimated using novel model at 1.5 T; it is also worth noting that the estimations using traditional model at 3 T had a large variability. However, the D^* reconstructed at

1.5 T with novel model was consistent and having better qualitative representation. Thus, the observation that D^* calculated using traditional model at 3 T could differentiate tumors against healthy PZ and BPH could be an artifactual finding, as was also observed by Merisaari et al. [41], suggesting further studies are needed to determine the role of D^* in a clinical setting.

ROC analysis has showed that D parameter obtained using novel model at 1.5 T was able to differentiate between tumor and healthy PZ (AUC: 0.98) with high sensitivity (94%) and specificity (94%), which is in agreement with literature [9, 42]. Whereas, D^* parameter using traditional model at 3 T showed higher AUC, which might be artifactual because of high noise in the parameter map. Parameter f and k (novel model at 1.5 T) have shown improvement in diagnostic performance while using novel model with high AUC (f: 0.76; k: 0.75), sensitivity (f: 63%; k: 100%), and specificity (f: 94%; k: 69%) in differentiation of tumor from healthy PZ.

Limitations

This study had few limitations including the same patients could not be scanned twice due to institutional ethical constraints and patients' permission; the patients imaged at 1.5 T were not the same patients scanned at 3 T. Thus, we could not assess the intra-modality repeatability and further work is needed to investigate this. Second, ROIs for tumor, healthy PZ and BPH were drawn manually by one radiologist, which may have led to biases in analysis. In future, automatic detection of different tissues could be employed. Third, in this study, sample size was relatively smaller limited to 32 patients and patients against Gleason score were not evenly distributed, which may not imply any firm conclusions for clinical applications. No correlation with clinical scores was performed as the number of patients with individual grade-wise PCa category was not large enough for any comprehensive analysis. Fourth, whole mount section histopathology was not available for all the subjects, as it is not performed at our institute as a standard procedure for all the patients undergoing radical prostatectomy. Fifth, parallel imaging acquisition may have affected SNR calculations of the dataset, given that SD was estimated from a background ROI. Lastly, analyses of the hybrid IVIM–DKI model performance with other DWI models (such as monoexponential, stretched exponential, kurtosis, or biexponential models) could not be compared, as was beyond the purpose of this study. This comparison of model performance could be very interesting and subject of future work, ideally using a larger patient cohort.

Conclusions

Total variation function-based optimization for IVIM–DKI model is proposed as a new analysis methodology. It was shown that even at lower field strength 1.5 T, using this novel model produced lower error in parameter estimation with better-quality parametric reconstruction and high diagnostic performance when compared with the traditional hybrid analysis method used at 3 T. IVIM–DKI could play an essential role in prostate lesion detection when used at 1.5 T (combined with a more advanced analysis method). Thus, IVIM–DKI can have a much broader application and impact on cancer management of the prostate diseases.

Declarations

Conflict of interest Authors declare that they have no competing interest with respect to this study.

References

1. Rebello RJ, Oing C, Knudsen KE, Loeb S, Johnson DC, Reiter RE, Gillessen S, Van der Kwast T, Bristow RG (2021) Prostate cancer. Nat Rev Dis Prim 7:1–27
2. Penzkofer T, Tempany-Afdhal CM (2014) Prostate cancer detection and diagnosis: the role of MR and its comparison with other diagnostic modalities—a radiologist's perspective. NMR Biomed 27:3–15
3. Ahmed HU, El-Shater Bosaily A, Brown LC, Gabe R, Kaplan R, Parmar MK, Collaco-Moraes Y, Ward K, Hindley RG, Freeman A, Kirkham AP, Oldroyd R, Parker C, Emberton M (2017) Diagnostic accuracy of multi-parametric MRI and TRUS biopsy in prostate cancer (PROMIS): a paired validating confirmatory study. Lancet 389:815–822
4. Mohler JL, Antonarakis ES, Armstrong AJ, D'Amico AV, Davis BJ, Dorff T, Eastham JA, Enke CA, Farrington TA, Higano CS, Horwitz EM, Hurwitz M, Ippolito JE, Kane CJ, Kuettel MR, Lang JM, McKenney J, Netto G, Penson DF, Plimack ER, Pow-Sang JM, Pugh TJ, Richey S, Roach M, Rosenfeld S, Schaeffer E, Shabsigh A, Small EJ, Spratt DE, Srinivas S, Tward J, Shead DA, Freedman-Cass DA (2019) Prostate cancer, version 2.2019. JNCCN J Natl Compr Cancer Netw 17:479–505
5. Turkbey B, Rosenkrantz AB, Haider MA, Padhani AR, Villeirs G, Macura KJ, Tempany CM, Choyke PL, Cornud F, Margolis DJ (2019) Prostate imaging reporting and data system version 2.1: 2019 update of prostate imaging reporting and data system version 2. Eur Urol 76:340–351
6. Döpfert J, Lemke A, Weidner A, Schad LR (2011) Investigation of prostate cancer using diffusion-weighted intravoxel incoherent motion imaging. Magn Reson Imaging 29:1053–1058
7. Shinmoto H, Tamura C, Soga S, Shiomi E, Yoshihara N, Kaji T, Mulkern RV (2012) An intravoxel incoherent motion diffusion-weighted imaging study of prostate cancer. Am J Roentgenol 199:496–500
8. Wang F, Wang Y, Zhou Y, Liu C, Xie L, Zhou Z, Liang D, Shen Y, Yao Z, Liu J (2017) Comparison between types I and II epithelial ovarian cancer using histogram analysis of monoexponential, biexponential, and stretched-exponential diffusion models. J Magn Reson Imaging 46:1797–1809
9. Tamura C, Shinmoto H, Soga S, Okamura T, Sato H, Okuaki T, Pang Y, Kosuda S, Kaji T (2014) Diffusion kurtosis imaging study of prostate cancer: preliminary findings. J Magn Reson imaging 40:723–729
10. Jambor I, Merisaari H, Taimen P, Boström P, Minn H, Pesola M, Aronen HJ (2015) Evaluation of different mathematical models for diffusion-weighted imaging of normal prostate and prostate cancer using high b-values: a repeatability study. Magn Reson Med 73:1988–1998
11. Le Bihan D, Breton E, Lallemand D, Aubin ML, Vignaud J, Laval-Jeantet M (1988) Separation of diffusion and perfusion in intravoxel incoherent motion MR imaging. Radiology 168:497–505
12. Jensen JH, Helpern JA, Ramani A, Lu H, Kaczynski K (2005) Diffusional kurtosis imaging: the quantification of non-Gaussian water diffusion by means of magnetic resonance imaging. Magn Reson Med 53:1432–1440
13. Lu Y, Jansen JFA, Mazaheri Y, Stambuk HE, Koutcher JA, Shukla-Dave A (2012) Extension of the intravoxel incoherent motion model to non-gaussian diffusion in head and neck cancer. J Magn Reson Imaging 36:1088–1096
14. Ianuş A, Santiago I, Galzerano A, Montesinos P, Loução N, Sanchez-Gonzalez J, Alexander DC, Matos C, Shemesh N (2020) Higher-order diffusion MRI characterization of mesorectal lymph nodes in rectal cancer. Magn Reson Med 84:348–364
15. Rudin LI, Osher S, Fatemi E (1992) Nonlinear total variation based noise removal algorithms. Phys D Nonlinear Phenom 60:259–268
16. Kayal EB, Kandasamy D, Khare K, Alampally JT, Bakhshi S, Sharma R, Mehndiratta A (2017) Quantitative analysis of intravoxel incoherent motion (IVIM) diffusion MRI using total variation and Huber penalty function. Med Phys 44:5849–5858
17. Kayal EB, Kandasamy D, Khare K, Bakhshi S, Sharma R, Mehndiratta A (2019) Intravoxel incoherent motion (IVIM) for response assessment in patients with osteosarcoma undergoing neoadjuvant chemotherapy. Eur J Radiol 119:108635
18. Malagi AV, Das CJ, Khare K, Calamante F, Mehndiratta A (2019) Effect of combination and number of b values in IVIM analysis with post-processing methodology: simulation and clinical study. Magn Reson Mater Phys Biol Med 32:519–527
19. Malagi AV, Kandasamy D, Khare K, Pushpam D, Kumar R, Bakhshi S, Mehndiratta A (2020) IVIM and diffusion Kurtosis MR Imaging on interim response assessment of Hodgkin Lymphoma. Proc Intl Soc Mag Reson Med 28:4870

20. Marques JP, Simonis FFJ, Webb AG (2019) Low-field MRI: an MR physics perspective. J Magn Reson Imaging 49:1528–1542

21. Wurnig MC, Kenkel D, Filli L, Boss A (2016) A standardized parameter-free algorithm for combined intravoxel incoherent motion and diffusion kurtosis analysis of diffusion imaging data. Invest Radiol 51:203–210

22. Fujima N, Sakashita T, Homma A, Yoshida D, Kudo K, Shirato H (2018) Utility of a hybrid IVIM-DKI model to predict the development of distant metastasis in head and neck squamous cell carcinoma patients. Magn Reson Med Sci 17:21–27

23. Fujima N, Yoshida D, Sakashita T, Homma A, Tsukahara A, Shimizu Y, Tha KK, Kudo K, Shirato H (2017) Prediction of the treatment outcome using intravoxel incoherent motion and diffusional kurtosis imaging in nasal or sinonasal squamous cell carcinoma patients. Eur Radiol 27:956–965

24. Suo S, Chen X, Wu L, Zhang X, Yao Q, Fan Y, Wang H, Xu J (2014) Non-Gaussian water diffusion kurtosis imaging of prostate cancer. Magn Reson Imaging 32:421–427

25. Lemke A, Stieltjes B, Schad LR, Laun FB (2011) Toward an optimal distribution of b values for intravoxel incoherent motion imaging. Magn Reson Imaging 29:766–776

26. Valerio M, Zini C, Fierro D, Giura F, Colarieti A, Giuliani A, Laghi A, Catalano C, Panebianco V (2016) 3T multiparametric MRI of the prostate: does intravoxel incoherent motion diffusion imaging have a role in the detection and stratification of prostate cancer in the peripheral zone? Eur J Radiol 85:790–794

27. Beyhan M, Sade R, Koc E, Adanur S, Kantarci M (2018) The evaluation of prostate lesions with IVIM DWI and MR perfusion parameters at 3T MRI. Radiol Med 124:1–7

28. Pesapane F, Patella F, Fumarola EM, Panella S, Ierardi AM, Pompili GG, Franceschelli G, Angileri SA, Magenta Biasina A, Carrafiello G (2017) Intravoxel incoherent motion (IVIM) diffusion weighted imaging (DWI) in the periferic prostate cancer detection and stratification. Med Oncol 34:1–9

29. Ertas M, Yildirim I, Kamasak M, Akan A (2013) Digital breast tomosynthesis image reconstruction using 2D and 3D total variation minimization. Biomed Eng Online 12:112

30. Dietrich O, Raya JG, Reeder SB, Reiser MF, Schoenberg SO (2007) Measurement of signal-to-noise ratios in MR images: influence of multichannel coils, parallel imaging, and reconstruction filters. J Magn Reson Imaging 26:375–385

31. Burnham KP, Anderson DR (2004) Multimodel inference: understanding AIC and BIC in model selection. Sociol Methods Res 33:261–304

32. Rosenkrantz AB, Oei M, Babb JS, Niver BE, Taouli B (2011) Diffusion-weighted imaging of the abdomen at 3.0 Tesla: image quality and apparent diffusion coefficient reproducibility compared with 1.5 Tesla. J Magn Reson Imaging 33:128–135

33. Saremi F, Jalili M, Sefidbakht S, Channual S, Quane L, Naderi N, Schultze-Haakh H, Torrone M (2011) Diffusion-weighted imaging of the abdomen at 3 T: image quality comparison with 1.5-T magnet using 3 different imaging sequences. J Comput Assist Tomogr 35:317–325

34. Beyersdorff D, Taymoorian K, Knösel T, Schnorr D, Felix R, Hamm B, Bruhn H (2005) MRI of prostate cancer at 1.5 and 3.0 T: comparison of image quality in tumor detection and staging. Am J Roentgenol 185:1214–1220

35. Ullrich T, Quentin M, Oelers C, Dietzel F, Sawicki LM, Arsov C, Rabenalt R, Albers P, Antoch G, Blondin D, Wittsack HJ, Schimmöller L (2017) Magnetic resonance imaging of the prostate at 1.5 versus 3.0 T: a prospective comparison study of image quality. Eur J Radiol 90:192–197

36. Mazaheri Y, Vargas HA, Nyman G, Akin O, Hricak H (2013) Image artifacts on prostate diffusion-weighted magnetic resonance imaging: trade-offs at 1.5 tesla and 3.0 tesla. Acad Radiol 20:1041–1047

37. Geethanath S, Vaughan JT (2019) Accessible magnetic resonance imaging: a review. J Magn Reson Imaging 49:e65–e77

38. Sasaki M, Yamada K, Watanabe Y, Matsui M, Ida M, Fujiwara S, Shibata E (2008) Variability in absolute apparent diffusion coefficient values across different platforms may be substantial: a multivendor, multi-institutional comparison study. Radiology 249:624–630

39. Lavdas I, Miquel ME, McRobbie DW, Aboagye EO (2014) Comparison between diffusion-weighted MRI (DW-MRI) at 1.5 and 3 tesla: a phantom study. J Magn Reson Imaging 40:682–690

40. Ding Y, Tan Q, Mao W, Dai C, Hu X, Hou J, Zeng M, Zhou J (2019) Differentiating between malignant and benign renal tumors: do IVIM and diffusion kurtosis imaging perform better than DWI? Eur Radiol. https://doi.org/10.1007/s00330-019-06240-6

41. Merisaari H, Movahedi P, Perez IM, Toivonen J, Pesola M, Taimen P, Boström PJ, Pahikkala T, Kiviniemi A, Aronen HJ (2017) Fitting methods for intravoxel incoherent motion imaging of prostate cancer on region of interest level: repeatability and gleason score prediction. Magn Reson Med 77:1249–1264

42. Cui Y, Li C, Liu Y, Jiang Y, Yu L, Liu M, Zhang W, Shi K, Zhang C, Zhang J (2019) Differentiation of prostate cancer and benign prostatic hyperplasia: comparisons of the histogram analysis of intravoxel incoherent motion and monoexponential model with in-bore MR-guided biopsy as pathological reference. Abdom Radiol 45:1–13